Immunity, Volume *49*

Supplemental Information

LAG-3 Inhibitory Receptor Expression Identifies Immunosuppressive Natural Regulatory Plasma Cells

Andreia C. Lino, Van Duc Dang, Vicky Lampropoulou, Anna Welle, Jara Joedicke, Jelka Pohar, Quentin Simon, Jessie Thalmensi, Aurelia Baures, Vinciane Flühler, Imme Sakwa, Ulrik Stervbo, Stefanie Ries, Luc Jouneau, Pierre Boudinot, Takeshi Tsubata, Takahiro Adachi, Andreas Hutloff, Thomas Dörner, Ursula Zimber-Strobl, Alex F. de Vos, Katja Dahlke, Gunnar Loh, Sarantis Korniotis, Christian Goosmann, Jean-Claude Weill, Claude-Agnès Reynaud, Stefan H.E. Kaufmann, Jörn Walter, and Simon Fillatreau

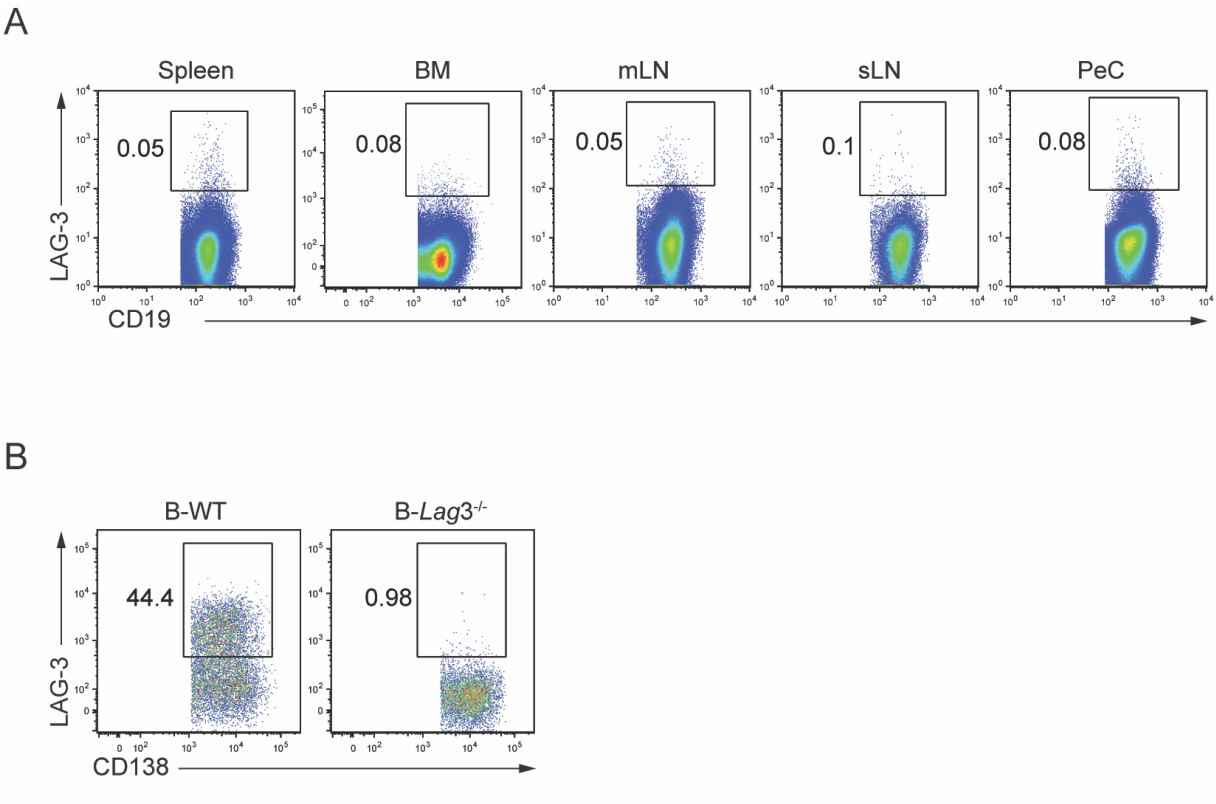

Figure S1: Expression of LAG-3 by B cells and plasmocytes in *Salmonella* infected mice, Related to Figure 1.

(A) Representative flow cytometry plots showing the expression of LAG-3 on $CD19^{+}CD138^{-}$ B cells from C57BL/6 mice in spleen, BM, mLN, sLN, and PeC on day 1 p.i. with *Salmonella* (SL7207, 10^7 CFU).

(B) Representative flow cytometry plots showing the expression of LAG-3 on splenic $CD138^{hi}$ cells of B-WT and B-*Lag3*$^{-/-}$ mice on day 1 p.i. with *Salmonella* (SL7207, 10^7 CFU).

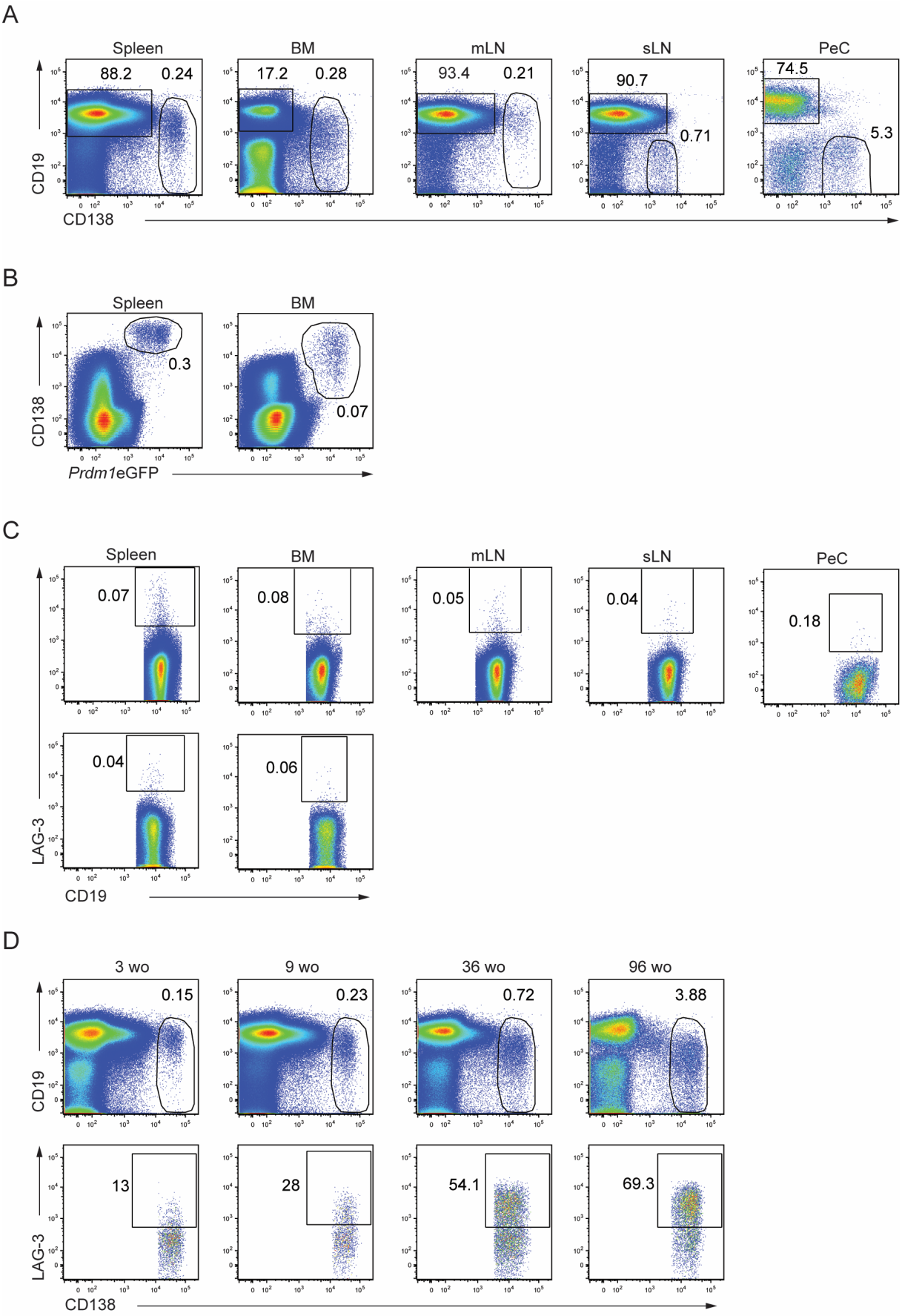
A
Spleen
BM
mLN
sLN
PeC
88.2
0.24
17.2
0.28
93.4
0.21
90.7
0.71
74.5
5.3
CD19
CD138
B
Spleen
BM
0.3
0.07
CD138
Prdm1eGFP
C
Spleen
BM
mLN
sLN
PeC
0.07
0.08
0.05
0.04
0.18
0.04
0.06
LAG-3
CD19
D
3 wo
9 wo
36 wo
96 wo
0.15
0.23
0.72
3.88
13
28
54.1
69.3
CD19
LAG-3
CD138

Figure S2: Presence of LAG-3-expressing plasma cells in naïve mice, Related to Figure 2.
(A) Representative flow cytometry plots showing the expression of CD19 and CD138 on live $CD4^-CD8^-$ lymphocytes in the indicated tissues. The gates identify $CD19^+CD138^-$ B cells characterized in Figure S2C, and $CD138^{+/hi}$ plasmocytes characterized in Figure 2A, for spleen, BM, mLN, sLN and PeC of naïve C57BL/6 mice.
(B) Representative flow cytometry plots showing the expression of CD138 and *Prdm1*eGFP on live $CD4^-CD8^-$ lymphocytes from spleen and BM of naïve *Prdm1*eGFP mice. The gates identify $CD138^{+/hi}$*Prdm1*$eGFP^+$ plasmocytes characterized in Figure 2B.
(C) Representative flow cytometry plots showing the expression of LAG-3 on $CD19^+CD138^-$ B cells in spleen, BM, mLN, sLN, and PeC from naïve C57BL/6 mice (top), as well as in spleen and BM from naïve *Lag3*$^{-/-}$ mice (bottom).
(D) Representative flow cytometry plots showing the expression of CD19 and CD138 in live $CD4^-CD8^-$ lymphocytes (top) and the expression of LAG-3 and CD138 in live $CD138^{hi}$ plasmocytes (bottom) from naïve C57BL/6 mice of indicated ages. The gates in top panels indicate $CD138^{hi}$ cells analysed for the expression of LAG-3 and CD138 in bottom panels.

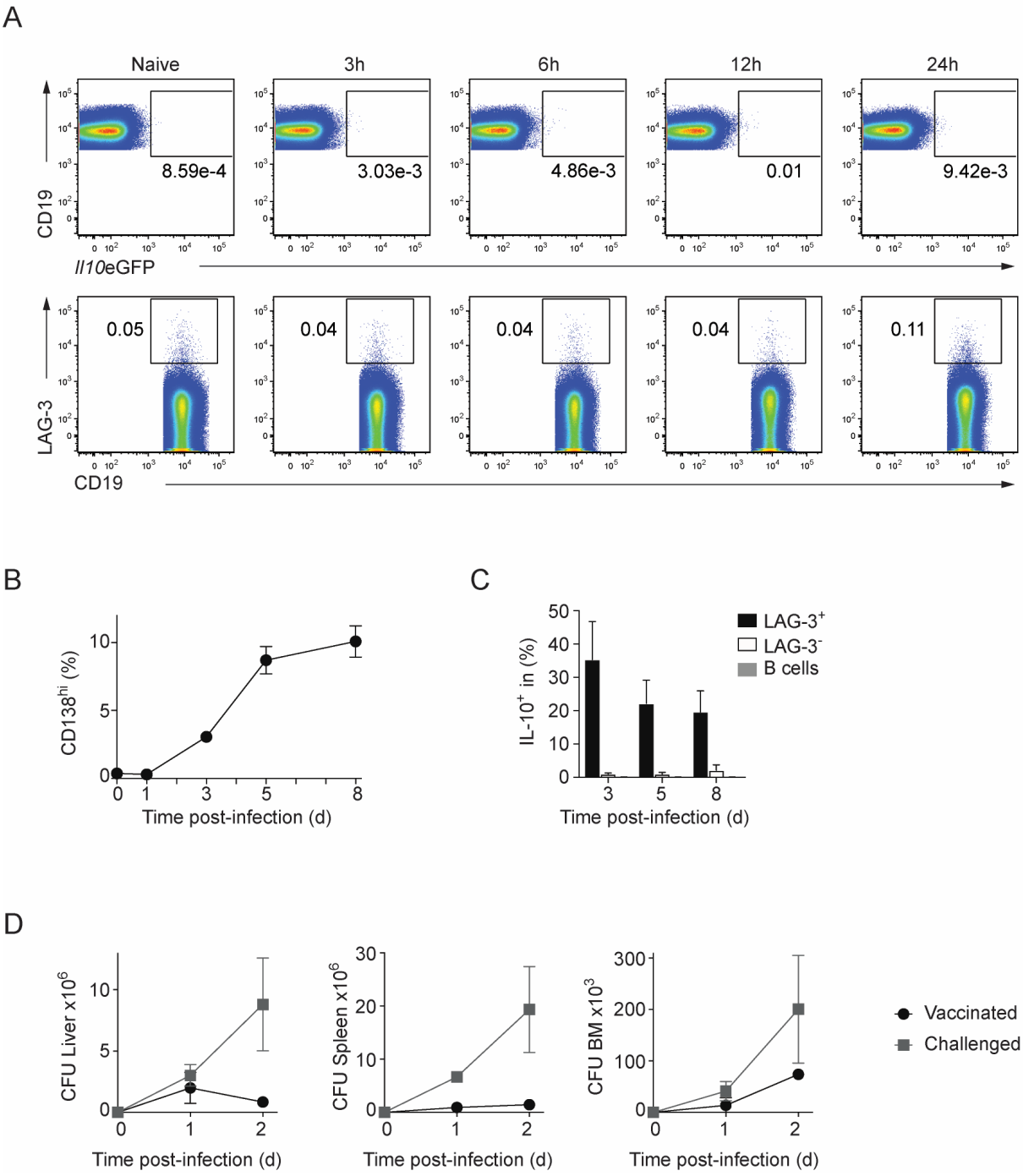
A
Naive
3h
6h
12h
24h
CD19
Il10eGFP
8.59e-4
3.03e-3
4.86e-3
0.01
9.42e-3
LAG-3
CD19
0.05
0.04
0.04
0.04
0.11
B
CD138hi (%)
Time post-infection (d)
C
IL-10+ in (%)
LAG-3+
LAG-3-
B cells
Time post-infection (d)
D
CFU Liver x10^6
CFU Spleen x10^6
CFU BM x10^3
Time post-infection (d)
Vaccinated
Challenged

Figure S3: Induction of IL-10 expression in LAG-3^{+}CD138^{hi} plasma cells during *Salmonella* infection, Related to Figure 3.

(A) *Il10*eGFP mice were challenged with *Salmonella* (SL7207, 10^7 CFU), and spleens were analysed at indicated hours p.i. Representative flow cytometry plots showing the expression of *Il10*eGFP and CD19 (top), and the expression of LAG-3 and CD19 (bottom) on live CD19^{+}CD138^{-} B cells.

(B) *Il10*eGFP mice were challenged with *Salmonella* (SL7207, 10^7 CFU). Data show the frequency of CD138^{hi} plasmocytes in CD4^{-}CD8^{-} live cells in spleen at indicated days p.i. Pool of two independent experiments with at least 6 mice per group.

(C) *Il10*eGFP mice were challenged with *Salmonella* (SL7207, 10^7 CFU), and spleens were analyzed at indicated days p.i. Data show frequencies of *Il10*eGFP^{+} cells in CD19^{+}CD138^{-} (B cells), LAG-3^{+}CD138^{hi} (LAG-3^{+}), and LAG-3^{-}CD138^{hi} (LAG-3^{-}) cells. Pool of two independent experiments with at least 6 mice per group

(D) *Il10*eGFP mice were vaccinated (SL7207, 10^6 CFU), and rechallenged 90 days later with *Salmonella* (SL7207, 10^7 CFU) together with naive age-matched control *Il10*eGFP mice. CFU were determined in liver (left), spleen (middle), and BM (right) at indicated days p.i. Data are pooled from two independent experiments with at least n=6 per group.

Data show mean ± SEM.

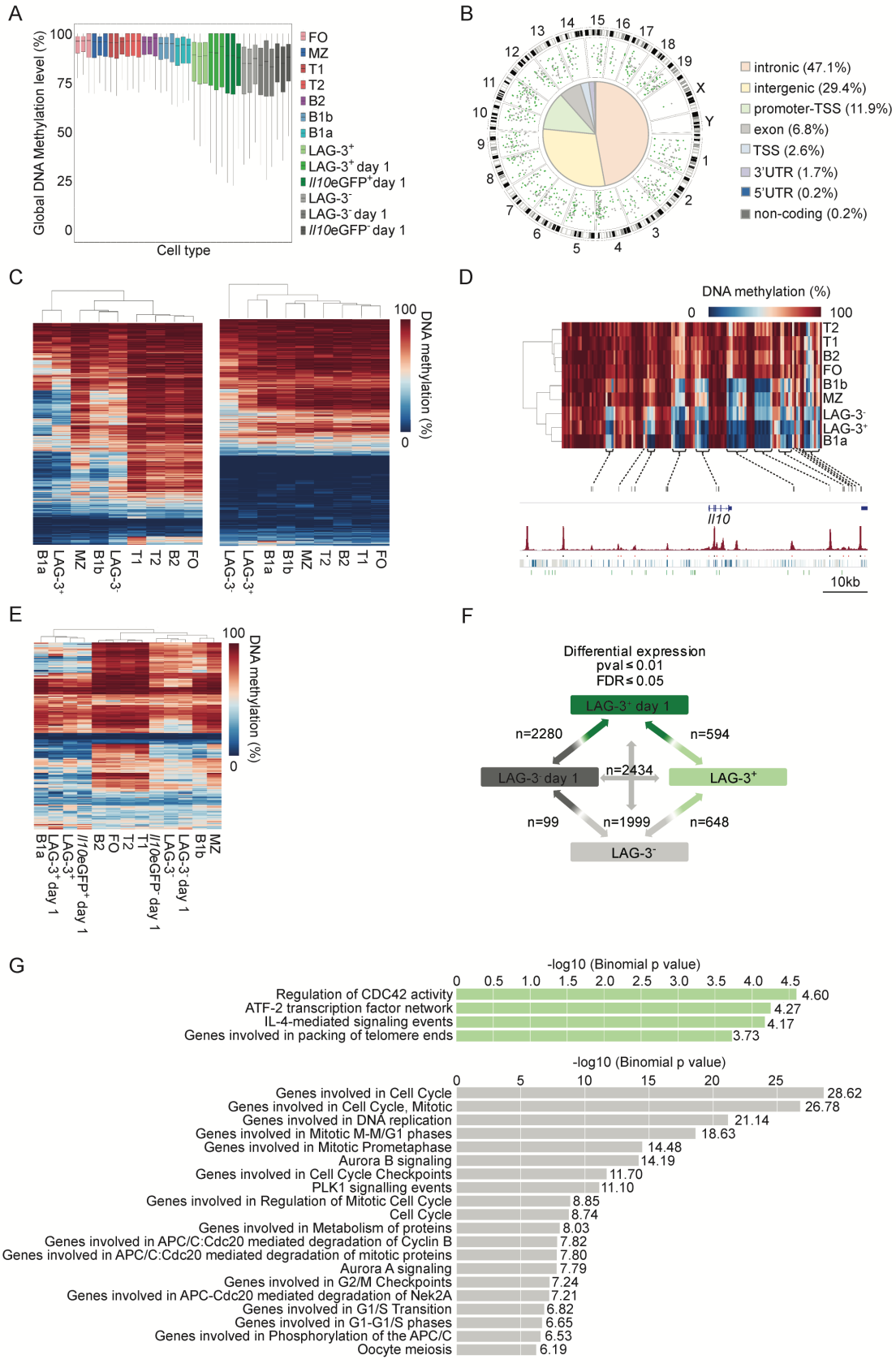
A
Global DNA Methylation level (%)
100
75
50
25
0
Cell type
FO
MZ
T1
T2
B2
B1b
B1a
LAG-3+
LAG-3+ day 1
Il10eGFP+day 1
LAG-3-
LAG-3- day 1
Il10eGFP- day 1
B
intronic (47.1%)
intergenic (29.4%)
promoter-TSS (11.9%)
exon (6.8%)
TSS (2.6%)
3'UTR (1.7%)
5'UTR (0.2%)
non-coding (0.2%)
C
DNA methylation (%)
100
0
B1a
LAG-3+
MZ
B1b
LAG-3-
T1
T2
B2
FO
D
DNA methylation (%)
0
100
T2
T1
B2
FO
B1b
MZ
LAG-3-
LAG-3+
B1a
Il10
10kb
E
DNA methylation (%)
100
0
B1a
LAG-3+ day 1
LAG-3+
Il10eGFP+ day 1
B2
FO
T2
T1
Il10eGFP- day 1
LAG-3-
LAG-3- day 1
B1b
MZ
F
Differential expression
pval ≤ 0.01
FDR ≤ 0.05
LAG-3+ day 1
n=2280
n=594
LAG-3- day 1
n=2434
LAG-3+
n=99
n=1999
n=648
LAG-3-
G
-log10 (Binomial p value)
0
0.5
1.0
1.5
2.0
2.5
3.0
3.5
4.0
4.5
Regulation of CDC42 activity 4.60
ATF-2 transcription factor network 4.27
IL-4-mediated signaling events 4.17
Genes involved in packing of telomere ends 3.73
-log10 (Binomial p value)
0
5
10
15
20
25
Genes involved in Cell Cycle 28.62
Genes involved in Cell Cycle, Mitotic 26.78
Genes involved in DNA replication 21.14
Genes involved in Mitotic M-M/G1 phases 18.63
Genes involved in Mitotic Prometaphase 14.48
Aurora B signaling 14.19
Genes involved in Cell Cycle Checkpoints 11.70
PLK1 signalling events 11.10
Genes involved in Regulation of Mitotic Cell Cycle 8.85
Cell Cycle 8.74
Genes involved in Metabolism of proteins 8.03
Genes involved in APC/C:Cdc20 mediated degradation of Cyclin B 7.82
Genes involved in APC/C:Cdc20 mediated degradation of mitotic proteins 7.80
Aurora A signaling 7.79
Genes involved in G2/M Checkpoints 7.24
Genes involved in APC-Cdc20 mediated degradation of Nek2A 7.21
Genes involved in G1/S Transition 6.82
Genes involved in G1-G1/S phases 6.65
Genes involved in Phosphorylation of the APC/C 6.53
Oocyte meiosis 6.19

Figure S4. Analysis of DNA methylation and gene expression, Related to Figure 4

(A) Boxplot showing the genome-wide methylation percentage for the indicated B lineage cell subsets.

(B) Circular representation showing the distribution of the 469 DMR identified between LAG-3^{+}CD138^{hi} cells and LAG-3^{-}CD138^{hi} cells from naïve mice across the chromosomes and the genome. The methylation frequency for each DMR is indicated for LAG-3^{+}CD138^{hi} cells (green dots) and LAG-3^{-}CD138^{hi} cells (grey dots). The genomic positions of the DMR on the chromosomes are given by their angular value, and their methylation ratio are indicated by their height from the centre (radius). The pie chart shows the global distribution of the DMR within functional genomic regions.

(C) Heat-maps displaying the methylation percentage of each CpG found in the 469 DMR (see Figure 4B) that are hypo-methylated (left) or hyper-methylated (right) in LAG-3^{+}CD138^{hi} cells compared to LAG-3^{-}CD138^{hi} cells.

(D) Heat-map showing the methylation ratio for all covered CpG positions in the *Il10* locus for the indicated B lineage cell subsets, and additional genomic information, as in Figure 4D. In addition, the location of Egr2 motifs is indicated by green bars.

(E) Heat-map displaying the methylation ratio for the DMR distinguishing LAG-3^{+}CD138^{hi} cells and LAG-3^{-}CD138^{hi} cells from naïve mice for the indicated B lineage cell subsets.

(F) Representation of the numbers of DEG (p-value $\leq$ 0.01 and FDR $\leq$ 0.05) for the indicated pairwise comparisons. The union of the ensembles of DEG contains 3631 elements.

(G) Gene set enrichment analysis for the DEG between LAG-3^{+}CD138^{hi} cells and LAG-3^{-}CD138^{hi} cells from naïve mice (MSigDB Pathway ontology). Upper and lower panels were obtained using the genes expressed at higher amounts in LAG-3^{+}CD138^{hi} cells, and LAG-3^{-}CD138^{hi} cells, respectively.

(B-E) Coverage weighted average methylation ratio from 3 replicates for each cell type are shown.

(A, E, F) All samples were from naïve mice except where indicated. (B, C, D, G) All samples were from naïve mice.

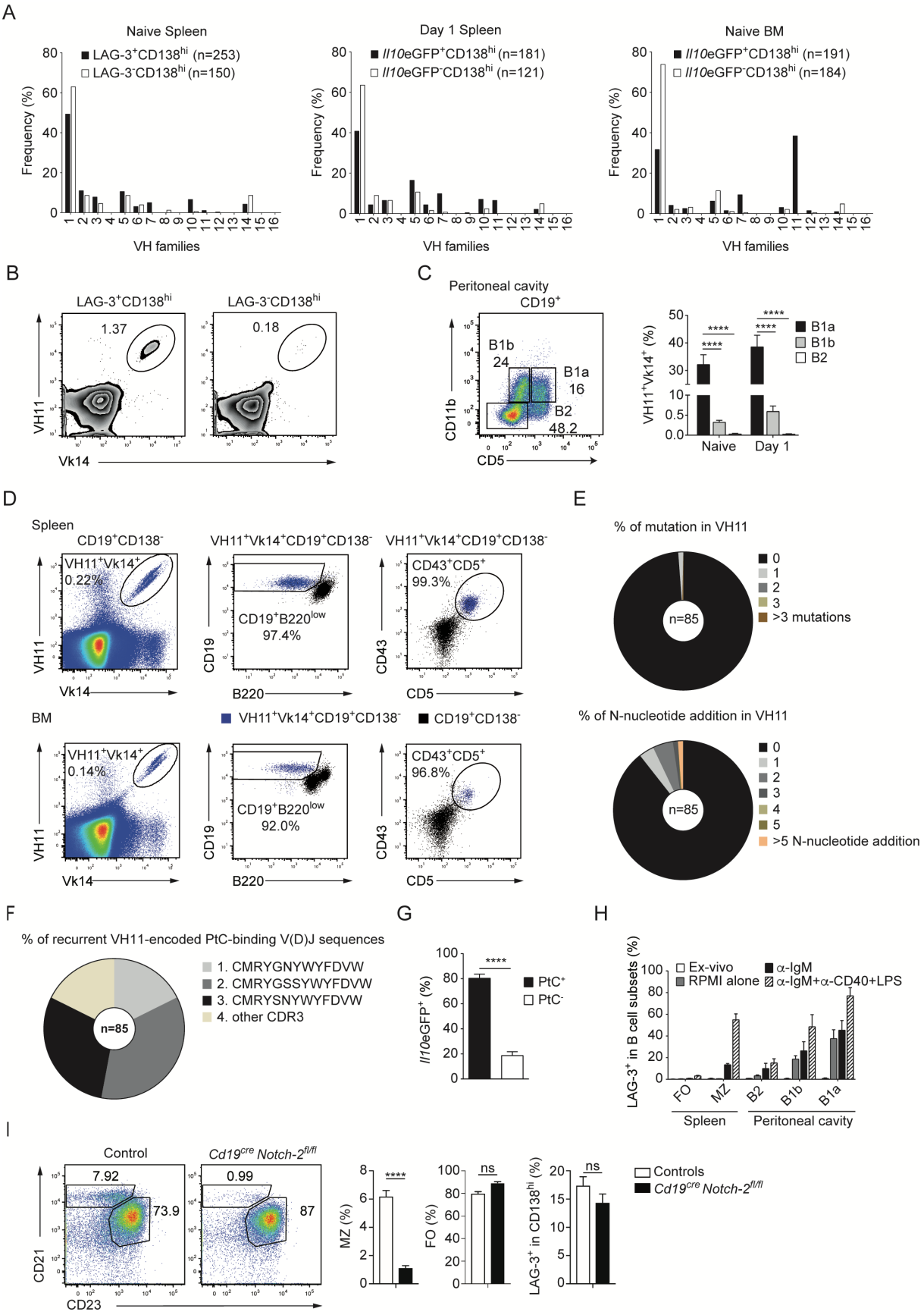
A
Naive Spleen
LAG-3+CD138hi (n=253)
LAG-3-CD138hi (n=150)
Day 1 Spleen
Il10eGFP+CD138hi (n=181)
Il10eGFP-CD138hi (n=121)
Naive BM
Il10eGFP+CD138hi (n=191)
Il10eGFP-CD138hi (n=184)
Frequency (%)
VH families
B
LAG-3+CD138hi
LAG-3-CD138hi
1.37
0.18
VH11
Vk14
C
Peritoneal cavity
CD19+
B1b
24
B1a
16
B2
48.2
CD11b
CD5
VH11+Vk14+ (%)
B1a
B1b
B2
Naive
Day 1
D
Spleen
CD19+CD138-
VH11+Vk14+CD19+CD138-
VH11+Vk14+
0.22%
CD19+B220low
97.4%
CD43+CD5+
99.3%
BM
VH11+Vk14+CD19+CD138-
CD19+CD138-
0.14%
92.0%
96.8%
E
% of mutation in VH11
n=85
0
1
2
3
>3 mutations
% of N-nucleotide addition in VH11
4
5
>5 N-nucleotide addition
F
% of recurrent VH11-encoded PtC-binding V(D)J sequences
1. CMRYGNYWYFDVW
2. CMRYGSSYWYFDVW
3. CMRYSNYWYFDVW
4. other CDR3
G
Il10eGFP+ (%)
PtC+
PtC-
H
LAG-3+ in B cell subsets (%)
Ex-vivo
RPMI alone
α-IgM
α-IgM+α-CD40+LPS
FO
MZ
B2
B1b
B1a
Spleen
Peritoneal cavity
I
Control
Cd19cre Notch-2fl/fl
7.92
73.9
0.99
87
CD21
CD23
MZ (%)
FO (%)
LAG-3+ in CD138hi (%)
ns
Controls
Cd19cre Notch-2fl/fl

Figure S5: BCR repertoire and antigen recognition properties of LAG-3- and IL-10-expressing plasmocytes, Related to Figure 5.

(A) Spleen LAG-3^{+}CD138^{hi} (naïve C57BL/6 mice, n=253) and LAG-3^{-}CD138^{hi} (naïve C57BL/6 mice, n=150), spleen *Il10*eGFP^{+}CD138^{hi} (day 1, n=181) and *Il10*eGFP^{-}CD138^{hi} (day 1, n=121), BM *Il10*eGFP^{+}CD138^{hi} (naïve, n=191) and *Il10*eGFP^{-}CD138^{hi} (naive, n=184) plasmocytes were isolated from naive and day 1-challenged mice (SL7207; 10^{7} CFU). Their *Igh* rearrangements were obtained by single cell PCR, and analysed using IMGT/V-Quest. Data show the IGHV family gene usage for the indicated populations.

(B) Representative flow cytometry plots showing the expression of VH11 and Vk14.126 on the indicated spleen cell populations from naïve (LAG-3^{+}CD138^{hi}, LAG-3^{-}CD138^{hi}) *Il10*eGFP mice.

(C) Representative flow cytometry plots showing the gating strategy to identify B1a (CD19^{+}CD11b^{+}CD5^{+}), B1b (CD19^{+}CD11b^{+}CD5^{-}) and B2 (CD19^{+}CD11b^{-}CD5^{-}) B cell subsets in PeC (gated on live CD19^{+} B cells). The histogram indicates the frequency of VH11^{+}Vk14.126^{+} among B1a, B1b and B2 subsets in naive and day 1-challenged *Il10*eGFP mice (SL7207, 10^{7} CFU). Data are pooled from 2 independent experiments (n=6 per time point).

(D) Representative flow cytometry plots showing the gating strategy to characterize VH11^{+}Vk14.126^{+} B1a cells in spleen (upper) and BM (bottom). Left plots show the expression of VH11 and Vk14.126 in CD19^{+}CD138^{-} B cells. Middle and right plots show the expression of CD19 and B220, as well as of CD43 and CD5, respectively, on VH11^{+}Vk14.126^{+}CD19^{+}CD138^{-} B cells from the spleen and BM of naïve C57BL/6 mice (in blue). The expression of these markers on CD19^{+}CD138^{-} B cells is indicated by the overlayed cells in black on the same plots. The percentages in the middle and right plots are the frequencies of CD19^{+}CD138^{-}VH11^{+}Vk14.126^{+} having the expression of CD19 and B220, as well as of CD43 and CD5, falling within the gates. Data is representative of 2 independent experiments.

(E) Frequency of IgH sequences having the indicated numbers of somatic mutations (top) or N-nucleotide additions (bottom) among all obtained VH11-positive sequences in spleen and BM from naïve and challenged mice.

(F) Frequency of IgH CDR3 sequences associated with PtC binding among all obtained VH11-positive IgH sequences in spleen and BM from naïve and challenged mice.

(G) Frequency of *Il10*eGFP^{+} cells within PtC- and non-PtC-reactive CD138^{hi} in BM from naive *Il10*eGFP mice. Data are pooled from 4 independent experiments (n=12).

(H) LAG-3 expression on B cell subsets *ex vivo*, and after overnight culture (RPMI, αIgM, αIgM+αCD40+LPS). Pools of 2-3 experiments.

(I) Flow cytometry plots and quantification of spleen B cell subsets in naïve *Cd19*-cre-*Notch2*$^{fl/f}$ mice (n=7) and littermate controls (pooled *Cd19*-cre and Notch2$^{fl/fl}$, n=8). Pool of 2 experiments (n=6).

Data show mean ± SEM. Results were compared using two-tailed unpaired t-test with Welch's correction in case of inequal variances (**** $p<0.0001$).

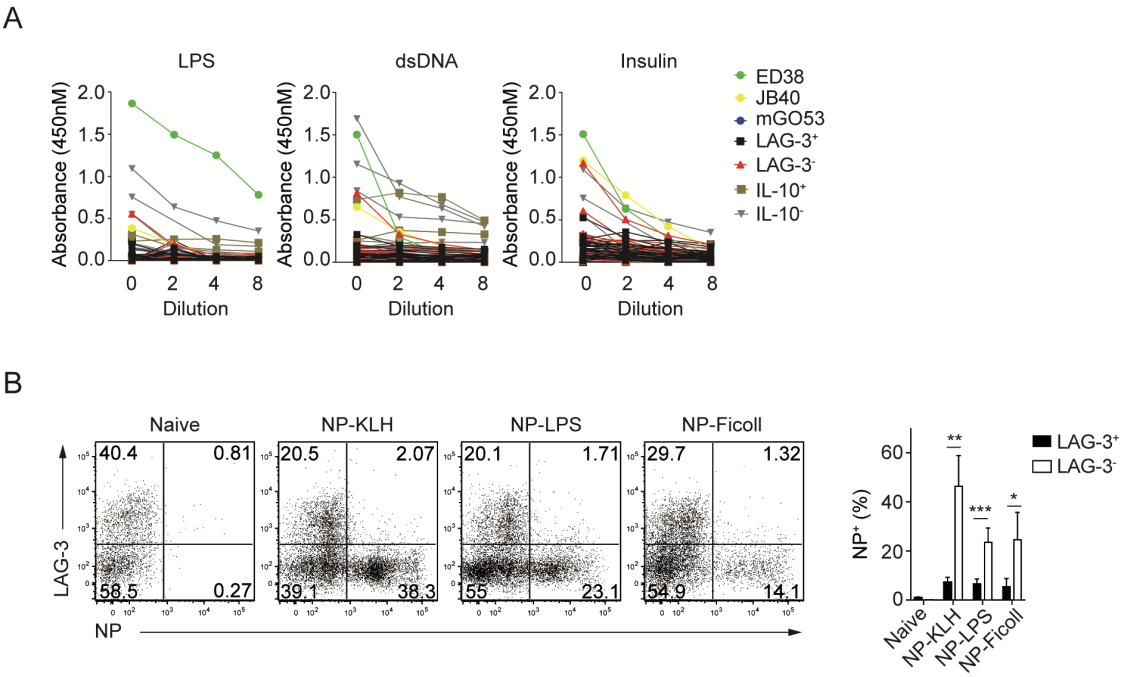

Figure S6: Reactivity of plasmocytes, Related to Figure 6.
(A) Reactivity of recombinant immunoglobulin from spleen LAG-3^{+} (n=25) and LAG-3^{-} (n=19), and BM *Il10*eGFP^{+} (n=6) as well as *Il10*eGFP^{-} (n=14) plasmocytes for LPS, dsDNA and insulin by ELISA. Green, yellow and blue lines are high positive ED38, low positive JB40, and negative control mGO53 antibodies, respectively.
(B) Flow cytometry plots showing binding of NP-allophycocyanin and expression of LAG-3 on CD138^{hi} cells from spleen of naïve and i.p. immunized mice (day 7 p.i.). Frequency of NP-binding cells within LAG-3^{+}CD138^{hi} and LAG-3^{-}CD138^{hi} spleen cells. Representative of 2 experiments (n=6). Data show mean ± SEM (*p<0.05, **p<0.01; *** p<0.001)

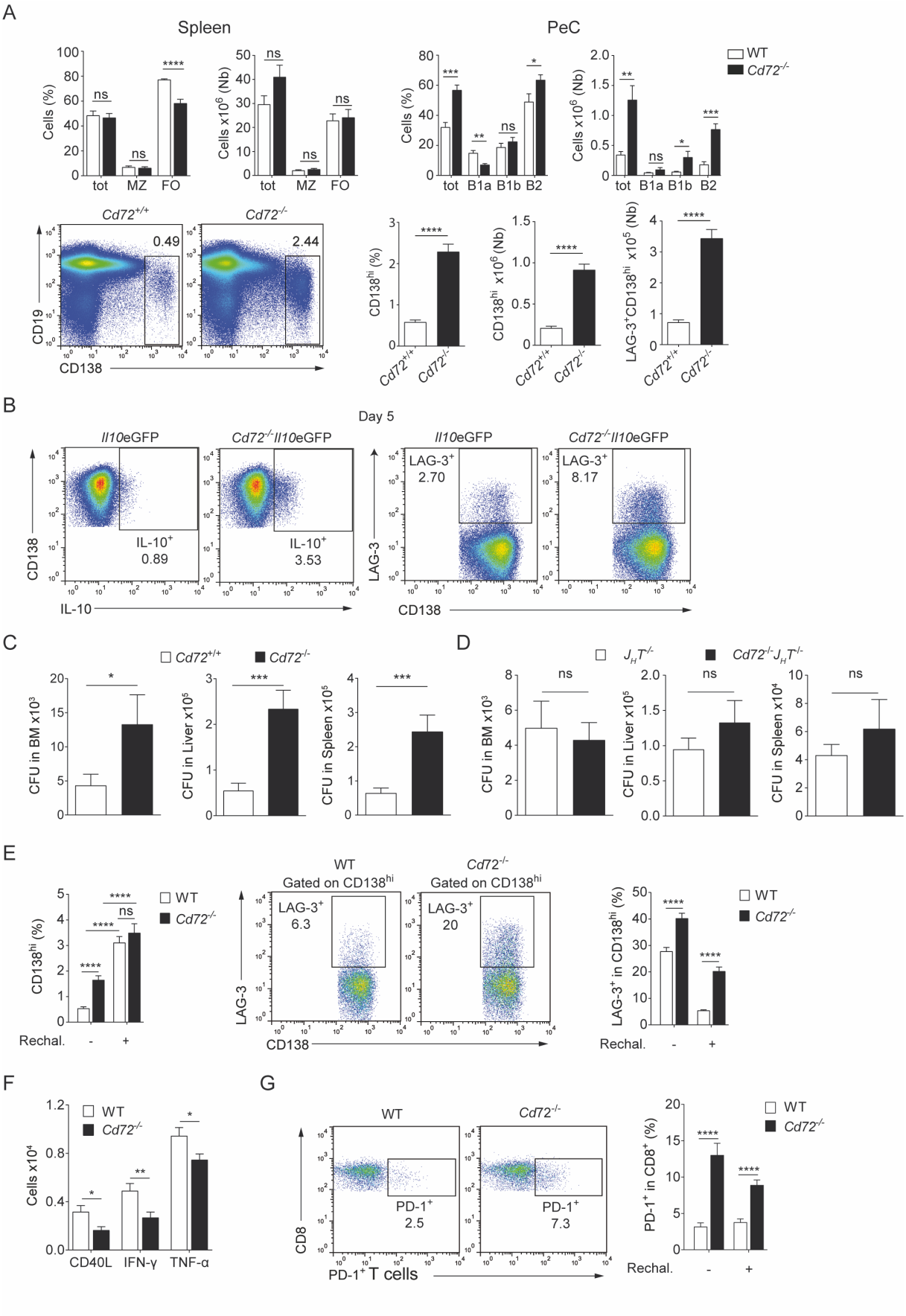
A
Spleen
PeC
WT
Cd72-/-
Cells (%)
Cells x10^6 (Nb)
tot
MZ
FO
B1a
B1b
B2
ns
Cd72+/+
Cd72-/-
0.49
2.44
CD19
CD138
CD138hi (%)
CD138hi x10^6 (Nb)
LAG-3+CD138hi x10^5 (Nb)
B
Day 5
Il10eGFP
Cd72-/-Il10eGFP
IL-10+
0.89
3.53
IL-10
LAG-3+
2.70
8.17
LAG-3
C
CFU in BM x10^3
CFU in Liver x10^5
CFU in Spleen x10^5
D
JHT-/-
Cd72-/-JHT-/-
CFU in BM x10^3
CFU in Liver x10^5
CFU in Spleen x10^4
E
CD138hi (%)
Rechal.
Gated on CD138hi
LAG-3+
6.3
20
LAG-3+ in CD138hi (%)
F
Cells x10^4
CD40L
IFN-γ
TNF-α
G
PD-1+
2.5
7.3
CD8
PD-1+ T cells
PD-1+ in CD8+ (%)

Figure S7: Host response of CD72-deficient mice during *Salmonella* infection, Related to Figure 7.
(A) Frequencies and numbers of total (tot) and indicated B cell subsets in spleen and PeC of naïve *Cd72*$^{-/-}$ and control mice. Pool of 2 experiments (n=6) (top). Flow cytometry plots and quantifications for CD138^{hi} and LAG-3^{+}CD138^{hi} cells in spleen of naïve *Cd72*$^{-/-}$ and littermate control. Pool of 3 experiments (n=13) (bottom).
(B) *Il10*eGFP and *Cd72*$^{-/-}$*Il10*eGFP shown in Figure 7A. Representative flow cytometry plots showing the expression of *Il10*eGFP and LAG-3 by CD138^{hi} cells at day 5 p.i. Data are representative from 3 independent experiments (n=9-12 per group).
(C) CFU on day 3 p.i. (SL1344, 100 CFU) for *Cd72*$^{-/-}$ and littermate controls. Pool of 5 experiments (n=22-25 per group)
(D) *Cd72*$^{-/-}$JHT (n=11) and JHT (n=10) mice were challenged with *Salmonella* (SL1344, 100 CFU). Data show CFU in BM, liver, and spleen on day 3 p.i. Data are pooled from 2 independent experiments.
(E) *Cd72*$^{-/-}$ and WT mice shown in Figure 7E. Histogram (left) shows the frequency of CD138^{hi} cells in spleen before (day 90) and 5 days after re-challenge. Representative flow cytometry plots show the expression of LAG-3 in spleen CD138^{hi} cells on day 5 after re-challenge (middle). Histogram (right) shows the frequency of LAG-3^{+} cells in CD138^{hi} cells in spleen on day 90 and day 5 after rechallenge.
(F) *Cd72*$^{-/-}$ and WT mice shown in Figure 7G. Numbers of CD40L-, IFN-γ-, and TNF-α-expressing *Salmonella*-reactive memory CD4^{+} T cells in BM on day 90 post-vaccination.
(G) *Cd72*$^{-/-}$ and WT mice shown in Figure 7H. Representative flow cytometry plots (day 95) and quantifications showing the frequency of PD-1^{+} cell in spleen CD8^{+} T cells on days 90 and 95.
Data show mean ± SEM. (^{ns}p > 0.05, *p<0.05, **p<0.01; **** p<0.0001).

Table S1. Top 50 genes that are higher expressed in naïve CD138^{hi}CD19^{+}LAG-3^{+} cells compared to naïve CD138^{hi}CD19^{+}LAG-3^{-} cells. Related to Figure 4.

Pvalue based top 50 genes that are higher expressed in naïve CD138^{hi}CD19^{+}LAG-3^{+} compared to naïve CD138^{hi}CD19^{+}LAG-3^{-}					
Rank	**Gene symbol**	**logFC**	**PValue**	**FDR**	**Synonyms**
1	Lag3	4.91	1.33E-07	0.001528	CD223|LAG-3|Ly66
2	Cpq	2.35	8.83E-07	0.002004	1190003P12Rik|2610034C17Rik|Hls2|Lal-1|Pgcp
3	Vav3	1.96	1.16E-06	0.002004	A530094I06Rik|AA986410|Idd18.1
4	Bcl2	1.67	1.4E-06	0.002004	AW986256|Bcl-2|C430015F12Rik|D630044D05Rik|D830018M01Rik
5	Zfp36l1	2.05	1.71E-06	0.002178	AW742437|AW743212|Berg36|Brf1|D530020L18Rik|ERF1|TIS11b|cMG1
6	Egr1	1.95	2.04E-06	0.002343	A530045N19Rik|ETR103|Egr-1|Krox-1|Krox-24|Krox24|NGF1-A|NGFI-A|NGFIA|TIS8|Zenk|Zfp-6|Zif268|egr
7	Inpp4a	1.89	3.49E-06	0.002981	107kDa|9630012D15|D130048C09Rik|R74740
8	Kctd12	1.45	3.66E-06	0.002981	AU046135|AW538430|Pfet1|Pfetin
9	Prg2	1.84	4.22E-06	0.002981	EMBP|MBP|mMBP|mMBP-1
10	Il4i1	2.70	4.59E-06	0.002981	Fig1|Fig1-ps|LAAO|LAO
11	Sema6d	1.91	4.65E-06	0.002981	1110067B02Rik|AA409156|D330011G23|mKIAA1479
12	Otud1	1.90	5.44E-06	0.003125	4933428L19Rik
13	Bcl2l15	1.96	6.53E-06	0.003273	Bfk|Gm566
14	Ppfibp2	1.45	6.68E-06	0.003273	Cclp1
15	Sirpa	1.32	7.47E-06	0.003273	AI835480|Bit|CD172a|P84|Ptpns1|SHP-1|SHPS-1|SIRP
16	Sell	2.59	7.49E-06	0.003273	AI528707|CD62L|L-selectin|LECAM-1|Lnhr|Ly-22|Ly-m22|Lyam-1|Lyam1
17	Jade2	1.31	8.61E-06	0.003273	1200017K05Rik|AI480685|Phf15|mKIAA0239
18	Krt222	1.45	9.23E-06	0.003273	6330509G02Rik
19	AW112010	1.97	9.69E-06	0.003273	-
20	Klf4	1.94	9.72E-06	0.003273	EZF|Gklf|Zie
21	Rgcc	1.52	1.04E-05	0.003273	1190002H23Rik|Rgc-32|Rgc32
22	Vegfa	2.01	1.06E-05	0.003273	Vegf|Vpf
23	Bhlhe40	2.58	1.08E-05	0.003273	Bhlhb2|C130042M06Rik|CR8|Clast5|Dec1|Sharp2|Stra13|Stra14
24	Ggh	2.00	1.18E-05	0.00346	gamma-GH
25	Oosp2	1.62	1.44E-05	0.003949	Gm99|Plac1l|Tmem122
26	Ly6k	1.67	1.48E-05	0.003951	2410015A16Rik|3110035B01Rik|mLy-6K
27	Cd200	1.65	1.77E-05	0.004608	Mox2|OX2
28	Serpina3f	1.45	2.06E-05	0.005062	2A1|BC049975
29	Plekha1	1.24	2.13E-05	0.005062	AA960558|C920009D07Rik|TAPP1
30	Nfkbiz	1.12	2.22E-05	0.005062	AA408868|INAP|Mail
31	Ackr3	1.92	2.25E-05	0.005062	AW541270|CXC-R7|CXCR-7|Cmkor1|Cxcr7|RDC-1|Rdc1
32	Rnf130	1.47	2.42E-05	0.005351	2510042A13Rik|G1RZFP|G1rp|GOLIATH|GP
33	Snn	1.14	2.87E-05	0.006151	2810407J07Rik|AI848521|AW547286
34	Egr2	2.55	0.00003	0.006272	Egr-2|Krox-20|Krox20|NGF1-B|Zfp-25|Zfp-6
35	Phlda1	1.47	3.24E-05	0.006652	DT1P1B11|TDAG51|Tdag
36	Il10	1.57	3.48E-05	0.006801	CSIF|Il-10
37	Ephx1	1.93	3.76E-05	0.007191	EH|Eph-1|Eph1|Epxh1|mEH
38	AB124611	1.49	5.07E-05	0.008396	Gm1706
39	Btla	1.34	0.000056	0.008941	A630002H24

40	Irf2bp2	1.15	5.77E-05	0.009071	E130305N23Rik|IRF-2BP2
41	Clec2i	1.80	5.85E-05	0.00908	Clr-g|Clrg|Dcl1|LCL-1|OCILrP2
42	Pglyrp1	1.31	6.71E-05	0.009416	PGRP|PGRP-S|Pglyrp|Tag7|Tasg7|Tnfsf3l
43	Abhd6	1.49	6.95E-05	0.009616	0610041D24Rik|AA673485|AV065425
44	Srsf7	0.89	0.000073	0.009846	35kDa|9430065L19Rik|9G8|NX-96|Sfrs7
45	Fgf1	3.38	7.36E-05	0.009846	Dffrx|Fam|Fgf-1|Fgfa
46	Ctss	1.32	0.000077	0.010022	Cats
47	Twsg1	1.26	7.88E-05	0.010022	1810013J15Rik|9030422N06Rik|AW552143|D17Ertd403e|Tsg|Twg
48	Zswim6	1.46	7.94E-05	0.010022	2900036G02Rik|mKIAA1577
49	Gpr18	1.49	8.27E-05	0.010103	-
50	Rtp4	1.62	8.39E-05	0.010104	5830458K16Rik|Ifrg28
Abbreviations					
LogFC		Log2 of fold change			
FDR		False Discovery Rate			

Table S2. Top 50 genes that are higher expressed in naïve CD138^{hi}CD19^{+}LAG-3^{-} cells compared to naïve CD138^{hi}CD19^{+}LAG-3^{+} cells. Related to Figure 4.

Pvalue based top 50 genes that are higher expressed in naïve CD138^{hi}CD19^{+}LAG-3^{-} compared to naïve CD138^{hi}CD19^{+}LAG-3^{+}					
Rank	**Gene symbol**	**logFC**	**PValue**	**FDR**	**Synonyms**
1	Ighe	-4.86	5.86E-07	0.002004	NA
2	Ighg3	-2.79	7.65E-07	0.002004	NA
3	Cdk1	-1.76	9.26E-07	0.002004	Cdc2|Cdc2a|p34<CDC2>
4	Mcm5	-1.81	1.25E-06	0.002004	AA617332|AI324988|AL033333|Cdc46|Mcmd5|P1-CDC46
5	Cdc45	-2.12	3.06E-06	0.002981	Cdc45l
6	Kpna2	-1.41	0.000004	0.002981	2410044B12Rik|IPOA1|PTAC58|Rch1
7	Ada	-1.14	4.83E-06	0.002981	-
8	Ighg2c	-3.01	4.93E-06	0.002981	NA
9	Eno1	-1.34	5.79E-06	0.003164	0610008I15|AL022784|Eno-1|MBP-1
10	Ncapg	-1.84	8.08E-06	0.003273	5730507H05Rik|Hcapg|MFT.M05.13
11	Rrm2	-1.63	8.94E-06	0.003273	AA407299|R2
12	Kif11	-1.64	9.79E-06	0.003273	Eg5|Kif8|Kifl1|Knsl1
13	Slpi	-2.10	9.81E-06	0.003273	-
14	Ighg2b	-2.66	1.03E-05	0.003273	NA
15	Ccnb2	-1.69	1.04E-05	0.003273	CycB2
16	Nuf2	-2.30	1.26E-05	0.003614	2410003C07Rik|AU044112|C85691|Cdca1|NUF2R
17	Cep55	-1.82	0.000014	0.003929	1200008O12Rik|2700032M20Rik
18	Spc24	-2.04	1.88E-05	0.004793	2410030K01Rik|AV109292|Spbc24
19	Rfc4	-1.21	0.000021	0.005062	A1|AI894123|AU040575|RFC37
20	Nmral1	-1.27	2.18E-05	0.005062	1110025F24Rik|AI256624
21	Ssr2	-1.57	2.89E-05	0.006151	1500032E05Rik|AI315033|AU020133|TLAP|TRAPB|TRAPbeta
22	Prelid1	-1.00	3.35E-05	0.006744	2610524G07Rik|Preli
23	Cdkn3	-1.82	3.49E-05	0.006801	2410006H10Rik|KAP
24	Cdc20	-1.83	4.37E-05	0.008221	2310042N09Rik|C87100|p55CDC
25	Tg	-1.33	4.74E-05	0.008396	Tgn|cog
26	Selm	-1.17	4.78E-05	0.008396	1500040L08Rik|A230103K18|Selm|Sepm
27	Ighv1-63	-2.70	4.86E-05	0.008396	NA
28	Ddost	-1.15	4.97E-05	0.008396	-
29	Ahcy	-1.19	5.06E-05	0.008396	AA987153|AL024110|CuBP|SAHH
30	Igkv4-69	-1.91	0.000051	0.008396	NA
31	NA	-3.48	5.12E-05	0.008396	NA
32	Ighv1-75	-4.83	5.12E-05	0.008396	NA
33	Top2a	-1.38	5.61E-05	0.008941	Top-2
34	Ighv15-2	-6.47	6.09E-05	0.009245	NA
35	Tigit	-1.83	6.12E-05	0.009245	ENSMUSG00000071552|Vstm3
36	H2-Eb1	-0.87	6.34E-05	0.009363	Eb|H-2Eb|H2Eb|Ia-4|Ia4
37	Spc25	-1.26	6.39E-05	0.009363	2600017H08Rik|2610205L13Rik|Spbc25
38	Kif22	-1.89	6.44E-05	0.009363	AU021460|C81217|Kid|Kif22a
39	Tcf19	-1.50	6.58E-05	0.009416	5730403J10Rik|AW495861
40	Mad2l1	-1.14	6.72E-05	0.009416	AA673185|MAD2
41	Cxcr3	-2.33	7.37E-05	0.009846	Cd183|Cmkar3
42	Igkv3-10	-1.93	7.74E-05	0.010022	NA
43	Pbk	-2.26	7.84E-05	0.010022	2810434B10Rik|AW538537|D14Ertd732e|TOPK
44	Ighv1-47	-5.14	8.04E-05	0.010035	NA
45	Dnpep	-1.03	8.16E-05	0.010078	AA407814

46	Srm	-0.92	0.000088	0.010211	AA407669|SpdST|SpdSy
47	Gstp2	-1.30	9.19E-05	0.010345	GSTpiA|Gst-3|Gst3
48	Tmem97	-1.47	9.61E-05	0.010583	1810014L12Rik|AI115531|AL022956|D11Bhm 182e
49	Shcbp1	-1.71	9.65E-05	0.010583	mPAL
50	Cenpe	-1.81	9.77E-05	0.010583	312kDa|AU019344|BC049989|C530022J18|CE NP-E|Kif10
Abbreviations					
LogFC		Log2 of fold change			
FDR		False Discovery Rate			

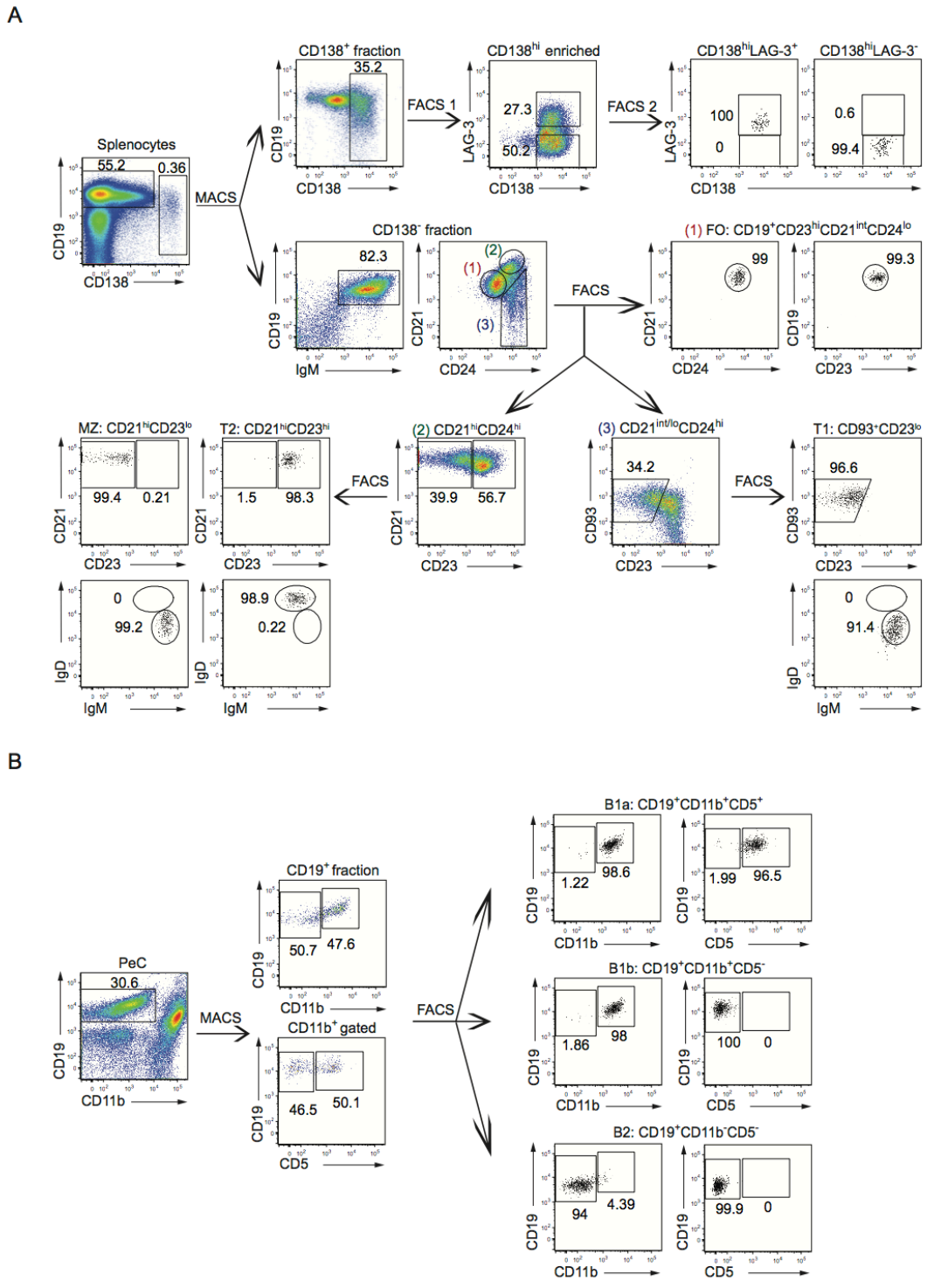

Methods S1: Strategy for the isolation of B lineage cell subsets, Related to STAR Methods
The isolation of spleen and PeC subsets are illustrated in panels A and B, respectively. For spleen, $CD138^+$ cells were first enriched by autoMACS after incubation with anti-CD138-PE (clone 281-2, BD Pharmingen) followed by anti-PE microbeads (Miltenyi Biotec). The $CD138^+$ fraction was then stained with anti-CD19, CD138, LAG-3, and CD11b/CD11c/CD3/PI. An additional enrichment of $CD138^{hi}$ cells was performed by flow cytometry sort (FACS 1), and $LAG\text{-}3^+CD138^{hi}CD11b^-CD11c^-CD3^-PI^-$ and $LAG\text{-}3^-CD138^{hi}CD11b^-CD11c^-CD3^-PI^-$ cells were then isolated by a second flow cytometry sort (FACS 2). Plasmocytes were isolated on

day 1 p.i. with 10^7 CFU *Salmonella* (SL7207) using the same strategy, according to LAG-3$^+$, LAG-3$^-$, *Il10*eGFP$^+$ and *Il10*eGFP$^-$ phenotypes. FMO controls were used to identify the LAG-3$^+$ and *Il10*eGFP$^+$ subsets. B cell subsets were isolated from the CD138$^-$ fraction obtained after autoMACS. First, T cells were depleted from the CD138$^-$ fraction by autoMACS. Follicular B cells (FO) (fraction 1 in the CD21 versus CD24 flow cytometry plot) were then isolated from this T cell-depleted CD138$^-$ fraction by flow cytometry as CD19$^+$CD23^{hi}CD21^{int}CD24^{lo}CD11b$^-$CD11c$^-$CD3$^-$PI$^-$ following staining with anti-CD19, CD21, CD23, CD24, CD11b/CD11c/CD3/PI. To obtain the other B cell subsets, the T cell-depleted CD138$^-$ fraction was stained with anti-CD19, IgM, IgD, CD21, CD23, CD24, CD93, and CD11b/CD11c/CD3/PI. Then, the fractions (2) CD19$^+$IgM$^+$CD21^{hi}CD24^{hi}CD11b$^-$CD11c$^-$CD3-PI$^-$ and (3) CD19$^+$IgM$^+$CD21$^{lo/int}$ CD24^{hi}CD11b$^-$CD11c$^-$CD3$^-$PI$^-$ were enriched by flow cytometry. The marginal zone (MZ) CD24^{hi}CD21^{hi}CD23^{lo} and transitional 2 (T2) CD24^{hi}CD21^{hi}CD23^{hi} were then sorted from fraction (2), and the transitional 1 (T1) CD24^{hi}CD21$^{lo/int}$CD23^{lo}CD93$^+$ from the fraction (3) by flow cytometry. For PeC, B cells were first purified by autoMACS via CD19-positive selection, then stained with anti-CD19, CD11b, CD5, CD11c, CD3, and PI. B1a: CD19$^+$CD11b$^+$CD5$^+$CD11c$^-$CD3$^-$PI$^-$; B1b: CD19$^+$CD11b$^+$CD5$^-$CD11c$^-$CD3$^-$PI$^-$ and B2: CD19$^+$CD11b$^-$CD5$^-$CD11c$^-$CD3$^-$PI$^-$ were then flow cytometry-sorted.